Multiple Group Search Optimization based on Decomposition for Multi-Objective Dispatch with Electric Vehicle and Wind Power Uncertainties

Xian Zhang[a], Ka Wing Chan[a,*], Huaizhi Wang[b], Bin Zhou[c,*], Guibin Wang[b], Jing Qiu[d]

[a] *Department of Electrical Engineering, The Hong Kong Polytechnic University, Hong Kong, 999077, China*

[b] *College of Mechatronics and Control Engineering, Shenzhen University, Shenzhen, 518060, China*

[c] *College of Electrical and Information Engineering, Hunan University, Changsha, 410082, China*

[d] *School of Electrical and Information Engineering, The University of Sydney, Australia*

Abstract— **While the number of plug-in electric vehicles (PEVs) increases rapidly, the application potential of PEVs should be accounted in electric power dispatch with several conflicting and competing objectives such as providing vehicle-to-grid (V2G) service or coordinating with wind power. To solve this highly constrained multi-objective optimization problem (MOOP), a multiple group search optimization based on decomposition (MGSO/D) is proposed considering the uncertainties of PEVs and wind power. Specifically, the decomposition approach effectively reduces the computational complexity, and the innovatively incorporated producer-scrounger model effectively improves the diversity and spanning of the Pareto-optimal front (PF). Meanwhile, the estimation error punishment is utilized to take into account of uncertainties. The performance of MGSO/D and the effectiveness of the uncertainty model are investigated on the IEEE 30-bus and 118-bus system with wind farms and PEV aggregators. Simulation results demonstrate the superiority of MGSO/D to solve this MOOP with practical uncertainties by comparing with well-established Pareto heuristic methods.**

Index Terms—**Multi-objective optimization, plug-in electric vehicles, multiple group search optimization based on decomposition, Pareto-optimal front.**

I. ACRONYMS

PEV	plug-in electric vehicle
V2G	vehicle-to-grid
MOOP	multi-objective optimization problem
MGSO/D	multiple group search optimization based on decomposition
PF	Pareto-optimal front

---

* Corresponding authors.

E-mail addresses: eekwchan@polyu.edu.hk (K. W. Chan), binzhou@hnu.edu.cn (B. Zhou)

MILP	a mixed integer linear programming
MOO	multi-objective optimization
GSO	group search optimization
NSGA-II	non-dominated sorting genetic algorithm-II
RE	renewable energy
SPEA	strength evolutionary algorithm
MOEA/D	multi-objective evolutionary algorithm based on decomposition
EA	evolutionary algorithm
PHEV	plug-in hybrid electric vehicles
VPP	virtual power plant
PDF	probability density function
DoD	depth of discharge
POZ	prohibited operating zone
ER	external repository

II. Introduction

Electric power dispatch is an important task in modern energy management systems to optimally allocate predicted system load among dispatchable generators with multiple competing objectives, such as economic operations, reliability, security and minimal impact on environment, subjected to transmission and operational constraints [41]. Over the years, research on multi-objective power dispatch has been extensively reported [24]. In conventional electric power dispatch, only thermal generators are concerned.

Due to the improvement of battery technologies, plug-in electric vehicles (PEVs) have developed rapidly in recent years and affected the traditional power dispatch in several aspects [1]. Fast growing uncontrolled PEV charging demand brings new pressure to the generation capacity of the power grid [3], raises the generation expansion cost [4], and lowers the generation economic efficiency [5]. Nevertheless, PEV batteries have potential to benefit the power system dispatch if properly controlled. For instance, causal charging could be shifted to valley load period to relief the requirement for peak generation [6]. Thanks to vehicle-to-grid (V2G) technologies [7-9], PEV batteries have more flexibilities to provide contributions to the system operation. In [8], an optimal dispatching strategy of V2G aggregator is developed to meet the driving demand of PEV owners and simultaneously maximize the economic income of aggregator. As presented in [9], PEVs with V2G can be utilized as portable power plant to improve the reliability and reserve of power systems as well as decrease the system dependencies on expensive units. In [10], a joint optimization model of generators and PEVs with V2G mode was presented to demonstrate the potential of PEVs to participate in power dispatch.

In addition, there will be a large penetration of renewable energies (REs) in future smart grids because of their advantages in reducing the pollution of conventional generators on the environment [11]. Therefore, in the electric power dispatch problem, the load should be allocated not only among conventional generators, but also among V2G power and REs. Due to the stochastic nature of PEVs and REs, the uncertainties in RE forecasting [44] and V2G power forecasting cannot be neglected in the power dispatch [17]. Optimal dispatch models accounting uncertainty of both REs and PEVs are formulated in [6],[17], but are not solved in a multi-objective manner. Microgrid operation scheduling framework with PEVs and REs is proposed and tackled by a mixed integer linear programming (MILP) based multi-objective optimization (MOO) method in [18], but the uncertainties of REs and EVs are not mentioned. After thoroughly reviewing the literature, it becomes evident that none of the previous studies has discussed the multi-objective power dispatch problem consider uncertainties of REs and V2G power. This paper therefore sets up an innovative multi-objective power dispatch model involved both REs and V2G power, which is modeled as a multi-objective optimization problem (MOOP). And in this model, the uncertainties of REs and V2G power are properly handled.

Furthermore, there are many barriers of applying the Pareto optimization algorithms into the MOOP with REs and PEVs. Weighted sum is a common approach [19] but many trials are claimed not efficient to obtain the non-convex PFs by adjusting the weights. Pareto-based MOO algorithms such as non-dominated sorting genetic algorithm-II (NSGA-II) [20] and strength evolutionary algorithm (SPEA) [21] have been utilized in the 2-objective MOOPs to achieve the compromise of fuel cost and air pollutants emission. A 2-objective MOOP considering uncertainties of REs and plug-in hybrid electric vehicles (PHEVs) is solved by NSGA-II in [22]. Nevertheless, broadening those algorithms to adapt more objectives for optimizations involving PEVs and REs is still insufficient. Group search optimization (GSO) is a recently proposed algorithm based on the producer-scrounger model inspired by animal searching behavior [23]. It was extended and improved to be a multi-objective GSO algorithm (MGSO) in [24] for large-scale MOOPs, which shows superiority in convergence and span metrics compared with NSGA-II and SPEA-II. Another up-to-date widely used algorithm is the multi-objective evolutionary algorithm (EA) based on decomposition (MOEA/D), which combines the advantages of weighted sum methods and EAs. It is proved that MOEA/D performs better than NSGA-II in many benchmark problems [25].

Under such background, a novel multi-objective power dispatch model considering uncertainties of V2G power and REs is proposed and a multiple group search optimization based on decomposition (MGSO/D) is developed to solve the highly constrained MOOPs with large dimension objectives in this paper. Compared with existing papers on similar topics, the main contributions of this paper are as follows: 1) The proposed MOOP is a multi-objective power dispatch problem with wind energy and V2G power penetration. Uncertainties of V2G power and wind power generators are considered in this problem. Specifically, the cost functions of wind generators and V2G power of EVs are derived according to the probability distributions

to study the probabilistic behaviors of REs and PEVs. 2) A novel algorithm called MGSO/D is developed to solve the proposed highly nonlinear constrained MOOP, which is inspired by the merits of the producer-scrounger model and decomposition. The MGSO/D explicitly decomposes the MOOP into several scalar subproblems [25], which leads the proposed algorithm to lower computational complexity at each generation. Then the subproblem is optimized based on the innovatively incorporated producer-scrounger model only using information of its several adjacent subproblems, thus the resulted PFs have better diversity and spanning metrics than other EAs.

III. THE MULTI-OBJECTIVE COMBINED POWER DISPATCH PROBLEM FORMULATION

A. Optimization Objectives Considering Uncertainties

The main goal of the electric power dispatch in modern energy management systems is to determine generation schedule with multiple competing objectives, such as "fuel cost", "emission reduction" and "energy saving", subjected to a set of operational and physical constraints [24][42]. Therefore, in this work, minimizing generation cost, emissions and power loss are selected as the three objective functions of the proposed power dispatch model corresponding to "fuel cost", "emission reduction" and "energy saving", respectively. In the objective of reducing generation cost, the estimation error punishment method [17][29] are utilized to coordinate the stochastic availability of V2G and wind power to reduce the loss resulted from uncertainties. In addition, the objective functions involved REs or PEVs are derived according to the probability density functions (PDFs) to account for their randomness.

1) Generation Cost Objective:

Because of the energy storage ability of PEV batteries, it is widely believed that PEVs could be coordinated dispatched to provide the V2G power to the power system [10] [17]. Due to the length limitation, this work would only focus on PEV power dispatch in the system operation while the PEV information interaction or market participation problems are not considered. All PEVs charged on the same bus are modeled as an aggregator and provides V2G power as a virtual power plant (VPP). On this premise, the uncertainties of V2G power as well as wind power are considered, and the battery degradation resulted by V2G is accounted.

Therefore, the economic objective f_1 is formulated in Eq. (1) to minimize the expected total generation cost, which is consisted of 3 parts: The first part denotes the cost summation of thermal generators while the second and third parts represent the cost of V2G power and the cost of wind power generators, respectively. PEV and wind power uncertainties are incorporated to this objective function.

$$f_1 = \sum_{k=1}^{N^{\mathrm{T}}} C_k^{\mathrm{T}}(T_k) + \sum_{n=1}^{N^{\mathrm{E}}} \left[C_n^{\mathrm{E}}(E_n) + C_n^{\mathrm{E,p}}(E_n^{\mathrm{AV}}, E_n) + C_n^{\mathrm{E,r}}(E_n^{\mathrm{AV}}, E_n) + C_n^{\mathrm{B}}(E_n) \right] + \sum_{m=1}^{N^{\mathrm{W}}} \left[C_m^{\mathrm{W}}(W_m) + C_m^{\mathrm{W,p}}(W_m^{\mathrm{AV}}, W_m) + C_m^{\mathrm{W,r}}(W_m^{\mathrm{AV}}, W_m) \right] \quad (1)$$

4

where N^{W}, N^{T} and N^{E} are the numbers of wind power generators, thermal generators, and nodes with V2G facilities installed; T_k is the active power generation of the kth thermal generator; C_k^{T} is the cost of the conventional generator; E_n and E_n^{AV} denotes the scheduled V2G power and actual available V2G output on node n; C_n^{E}, $C_n^{\mathrm{E,p}}$ and $C_n^{\mathrm{E,r}}$ are the V2G direct operation cost, underestimated penalty cost and overestimated penalty cost; C_n^{B} is the battery degradation cost; W_m and W_m^{AV} are the scheduled and the actual available output of wind generator m; C_m^{W}, $C_m^{\mathrm{W,p}}$ and $C_m^{\mathrm{W,r}}$ are the direct cost, underestimated penalty cost and overestimated penalty cost of the mth wind generator, respectively. It can be observed in (1) that the active power outputs, penalties, and cost coefficients are the key factors determining the generation cost.

The first component (thermal generation cost) is non-convex because of the valve-point effects, which could be modeled by ripple curves [26]. Therefore, the cost function for a conventional generator is represented as a combination of a quadratic function and a sine component term:

$$C_k^{\mathrm{T}}(T_k) = a_k T_k^2 + b_k T_k + c_k + | d_k \sin[e_k (T_k^{\min} - T_k)] | \tag{2}$$

where a_k, b_k, c_k, d_k and e_k are cost coefficients for the kth conventional generator. $T_k^{\min}$ is the minimum active power output of the kth thermal generator.

The second component (cost of V2G power) is divided into four parts, including $C_n^{\mathrm{E}}(E_n)$, $C_n^{\mathrm{E,p}}(E_n^{\mathrm{AV}}, E_n)$, $C_n^{\mathrm{E,r}}(E_n^{\mathrm{AV}}, E_n)$ and $C_n^{\mathrm{B}}(E_n)$ [10][27-28]. The first part is the scheduled power direct cost $C_n^{\mathrm{E}}(E_n)$:

$$C_n^{\mathrm{E}}(E_n) = g_n^{\mathrm{E}} E_n \tag{3}$$

where g_n^{E} represents coefficients of direct operation cost.

Based on the conclusion of [18], the PDF of the actual V2G power $f_P(E_n^{\mathrm{AV}})$ is assumed a normal distribution:

$$f_P(E_n^{\mathrm{AV}}) = (1 / \sqrt{2\pi\phi^2}) \cdot \exp[(E_n^{\mathrm{AV}} - \mu)^2 / (2\phi^2)] \tag{4}$$

where μ and ϕ are the mean and standard deviation of the normal distribution, respectively. Studies such as [46] indicate the uncertainties of V2G power are related to the factors of EV availability, trip durations, time of trips, et al, but such details are ignored in this work as the Jarque-Bera (JB) normality test and the P-values calculation carried out in [17] have verified that the assumption of normal distribution is precisely enough for the modeling of V2G power uncertainty.

Because the outputs of V2G power are highly stochastic, the system power dispatch based on the forecasted data will have deviations [45]. If the scheduled power is less than the available power, surplus power has to be wasted. On the other hand, if the scheduled power is more than the available power, reserve service is needed to compensate this imbalance. According to the PDF in Eq. (4) and this estimation error punishment principle, the second and third parts, underestimated penalty cost $C_n^{\mathrm{E,p}}(E_n^{\mathrm{AV}}, E_n)$ and overestimated penalty cost $C_n^{\mathrm{E,r}}(E_n^{\mathrm{AV}}, E_n)$, are derived as

$$C_n^{\mathrm{E,p}}(E_n^{\mathrm{AV}}, E_n) = \varepsilon_n^{\mathrm{E,p}} \int_{E_n}^{+\infty} (E_n^{\mathrm{AV}} - E_n) f_P(E_n^{\mathrm{AV}}) dE_n^{\mathrm{AV}} = \frac{\varepsilon_n^{\mathrm{E,p}}}{2}(\mu - E_n)[1 + erf(\frac{\mu - E_n}{\sqrt{2}\phi}) + \frac{\varepsilon_n^{\mathrm{E,p}} \cdot \phi}{\sqrt{2\pi}} e^{\frac{-(\mu - E_n)^2}{2\phi^2}}] \tag{5}$$

$$C_n^{E,r}\left(E_n^{AV},E_n\right)=\varepsilon_n^{E,r}\int_0^{E_n}\left(E_n^{AV}-E_n\right)f_P\left(E_n^{AV}\right)dE_n^{AV}=(\varepsilon_n^{E,r}\cdot\phi/\sqrt{2\pi})\{\exp(\frac{-\mu^2}{2\phi^2})-\exp[\frac{-(\mu-E_n)^2}{2\phi^2}]\}$$

$$+(\varepsilon_n^{E,r}/2)(\mu-E_n)\{erf[\mu/(\sqrt{2}\phi)]-erf[(\mu-E_n)/(\sqrt{2}\phi)]\}\tag{6}$$

where $erf(\cdot)$ represents the Gauss error function, which could be calculated with numerical integration; $\varepsilon_n^{E,p}$ and $\varepsilon_n^{E,r}$ represent coefficients of underestimated penalty and overestimated penalty cost of the V2G power on node n, respectively.

Providing V2G power by PEVs will accelerate the battery degradation, the cost of which could be calculated in proportion to the V2G power. Besides, additional compensation should be paid to motivate PEV owners to participate in the V2G service. Hence the fourth part, total degradation cost $C_n^B(E_n)$, should be set higher than the direct battery degradation cost:

$$C_n^B(E_n)=(1+r)[C^{BI}/(1000L^C E^B d^{DOD})]E_n\tag{7}$$

where r is the PEV aggregator operation cost coefficient for additional compensation; C^{BI} denotes the battery investment cost; L^C corresponds to PEV's battery cycle life at a certain depth of discharge (DoD); E^B represents PEV's battery capacity; d^{DOD} is the DoD to determine L^C; the number 1000 is applied to convert the kWh to MWh.

Similarly, the cost of a wind power generator consists of 3 parts, C_m^W, $C_m^{W,p}$ and $C_m^{W,r}$. The direct cost C_m^W is:

$$C_m^W(W_m)=g_m^W W_m\tag{8}$$

where g_m^W denotes the coefficient of direct cost. C_m^W accounts the cost paid by system operator to the wind power owners. It should be noted that C_m^W is 0 if the generators are owned by the system operator because the incremental cost of wind power is 0. As stated before, the underestimation and overestimation of wind power will lead to additional losses. Considering this uncertainty, the expectations of the underestimated penalty cost $C_m^{W,p}(W_m^{AV},W_m)$ and overestimated penalty cost $C_m^{W,r}(W_m^{AV},W_m)$ are derived as [29]:

$$C_m^{W,p}\left(W_m^{AV},W_m\right)=\varepsilon_m^{W,p}\int_{W_m}^{w_m^r}\left(W_m^{AV}-W_m\right)f_W\left(W_m^{AV}\right)dW_m^{AV}\tag{9}$$

$$C_m^{W,r}\left(W_m^{AV},W_m\right)=\varepsilon_m^{W,r}\int_0^{W_m}\left(W_m^{AV}-W_m\right)f_W\left(W_m^{AV}\right)dW_m^{AV}\tag{10}$$

where $\varepsilon_m^{W,p}$ and $\varepsilon_m^{W,r}$ denote coefficients of underestimated penalty and overestimated penalty cost for the mth wind generator. w_m^r is the rated wind power of the mth wind generator and $f_W(W_m^{AV})$ corresponds to the PDF of wind power, which can be described as follows [29]:

$$f_W\left(W_m^{AV}\right)=\frac{\gamma l v_m}{h}[\frac{(1+\rho l)v_m}{h}]^{\gamma-1}\exp\{-[\frac{(1+\rho l)v_m}{h}]^\gamma\}\tag{11}$$

where v_m is the wind speed of the mth wind generator, h and γ accounts for the scale factor and sharp factor at a given location, l denotes the ratio of linear range of wind speed to cut-in wind speed and ρ represents the ratio of wind power output to the rated wind power. Compared with (11), the bivariate normal distribution [29] could describe the uncertainty of wind power more

precisely. The bivariate normal distribution supposes 2 independent random variables for wind uncertainty, each of which has the standard normal distribution. Thus 5 parameters are needed, which are the mean and standard deviation of each normal distribution, and the cross correlation between the 2 variables. The 2-parameter (h and γ) distribution described in (11) is less complicated than the 5-parameter bivariate normal distribution, but it has been proved to provide a good fit to the observed wind power data [29]. Meanwhile, if the 2 parameters are known at one height, the corresponding parameters can be easily adjusted by a consistent methodology to another desired height [47]. It should be noted that the integration results could be easily obtained by the quadrature methods.

2) *Emission Objective*

Sulfur oxides and nitrogen oxides exhausted from thermal generators are the most important emissions considered in the power generation industry, which would cause serious air pollution. Therefore, the second objective aims to reduce these emissions from thermal power plants. The overall emission in ton/h could be formulated as [30]

$$f_2 = \sum_{k=1}^{N^{\mathrm{T}}} 10^{-2} \left(\alpha_k T_k^2 + \beta_k T_k + \zeta_k + \chi_k \exp(\lambda_k T_k) \right) \tag{12}$$

where α_k, β_k, ζ_k, χ_k and λ_k are the emission coefficients of the kth thermal generator. In (12), T_k is the independent variable, which represents the active power generation of the kth thermal generator. And the polynomial function ($\alpha_k T_k^2 + \beta_k T_k + \zeta_k$) represents sulfur oxides emissions and the exponential function ($\chi_k \exp(\lambda_k T_k)$) corresponds to nitrogen oxides emissions.

3) *Power Loss Objective*

The third objective is to reduce the system power loss. The goal is to minimize the real power loss in transmission lines, which could be solved using Newton-Raphson method and derived as follows [43]:

$$f_3 = P^{\mathrm{LOSS}} = \sum_{ij=1}^{N^{\mathrm{L}}} G_{ij}(V_i^2 + V_j^2 - 2V_i V_j \cos(\delta_i - \delta_j)) \tag{13}$$

where N^{L} represents the number of transmission lines. V_i, V_j are respectively the voltage magnitude of bus i and bus j. δ_i and δ_j denote the voltage angle of node i and node j, and G_{ij} corresponds to the conductance of the line between node i and j. V_i, V_j, δ_i and δ_j are dependent variables while active power generation for the kth thermal generator, nth V2G power and mth wind power generator (T_k, E_n and W_m) are independent variables mentioned in the first two objectives. The solution of P^{LOSS} involves the calculation of load flow problem and the derivation process can be found in [43]. Meanwhile, the system total power loss would depend on the network voltage, topology, line parameters, and load distributions of the system, etc.

B. *Multi-objective Optimization Problem Constraints*

1) *Power Balance Constraints:*

Power balance equality constraint indicates that the total electric power generation from thermal units, wind power and V2G

7

power should be equal to the total power loss P^{LOSS} plus the total load P^{D}:

$$\sum_{k=1}^{N^{\text{T}}}T_k + \sum_{m=1}^{N^{\text{W}}}W_m + \sum_{n=1}^{N^{\text{E}}}E_n - P^{\text{D}} - P^{\text{LOSS}} = 0 \tag{14}$$

This constraint could be satisfied by redistributing the total active power output after the power flow calculation.

2) *Transmission Line Apparent Power Constraints:*

This constraint is to guarantee that the apparent power of the transmission line from bus i to j (and j to i) S_{ij} (and S_{ji}) should be limited within its maximum loading capacity $S_{ij,max}$ for secure operation of transmission system. It can be formulated as:

$$\max[|\,S_{ij}\,|,|\,S_{ji}\,|] \le S_{ij,\max} \quad ij = 1,2,...,N^{\text{L}} \tag{15}$$

3) *Generation Capacity Constraints*

In practice, thermal generators have prohibited operating zones (POZs) because of the physical constraints of power plant components (e.g. shaft bearing tremor is magnified in some operating zones) [31]. For a POZ, the generator could only operate below or above this zone. These disconnected sub-zones form a non-convex decision space and make the proposed MOOP highly nonsmoothed, non-continuous and nonlinear. The output delivered by the kth generator while considering POZ is given in (16).

$$\begin{cases} T_k^{\min} \le T_k \le T_{k,1}^{ub} \\ T_{k,u-1}^{lb} \le T_k \le T_{k,u}^{ub}, u = 2,3,...,NP_s \\ T_{k,u}^{lb} \le T_k \le T_k^{\max}, u = NP_s \end{cases} \tag{16}$$

where $T_k^{\min}$, $T_k^{\max}$ are the minimum and maximum active output power of kth generator. $T_{k,u}^{lb}$ and $T_{k,u}^{ub}$ represent the lower and upper limits of the kth generator with uth POZ, and NP_s corresponds to the number of POZ of kth generator.

Besides, the generation capacity limits of the scheduled V2G power and wind power are stated as:

$$E_n^{\min} \le E_n \le E_n^{\max} \tag{17}$$

$$W_m^{\min} \le W_m \le W_m^{\max} \tag{18}$$

where E_n^{min} and E_n^{max} account for the lower and upper bound of the scheduled V2G power n while W_n^{min} and W_n^{max} account for the lower and upper limits of the scheduled wind power m.

C. An Extended Multi-Period Multi-Objective Optimal Dispatch Model

Although this work mainly focuses on the single-period multi-objective power dispatch model, which belongs to the category of so-called *economic dispatch* problems, an extension of the proposed model to multi-period problems is necessary for the following several reasons: Firstly, some constraints cannot be considered in the single-period model, such as the PEV charging/ discharging characteristics and generator ramp rate constraints. Secondly, an extended multi-period model is helpful to

8

account for the interrelations among PEVs, thermal generators and wind power generators. Thirdly, the environmental cost for charging PEVs can be better accounted in the multi-period model.

It is worth pointing out that emissions associated with PEVs, which are in fact the emissions of power generation of thermal generators for charging, could be considered in the multi-period model. The V2G power is generated from the electricity stored in the batteries of PEVs, which could be supplied by the thermal generators and other generators in the other periods. Therefore, the emission objective is a function of active power generation of thermal generators in the multiple periods, which can account for the quantity in other periods corresponding to the former charge cycles.

Based on the proposed model, a multi-period multi-objective optimal dispatch model is formulated as follows:

1) *Multi-period multi-objectives:*

$$\text{Minimize} \qquad \left\{ \sum_{t\in\Omega_T} f_1^t, \quad \sum_{t\in\Omega_T} f_2^t, \quad \sum_{t\in\Omega_T} f_3^t \right\} \qquad t\in\Omega_T \tag{19}$$

The multi-objective functions f_1, f_2 and f_3 are the same with Eq. (1), Eq. (12) and Eq. (13), but are extended to multi-period by the summation of each objective over different periods. And Ω_T is the multi-period set.

2) *Additional Multi-period Constraints:*

Some additional constraints can be considered in the multi-period model. (20) states the generator ramp rate constraints.

$$-R_{down,k} \leq T_k^t - T_k^{t-1} \leq R_{up,k} \qquad \forall t \in \Omega_T \tag{20}$$

where $R_{down,k}$ and $R_{up,k}$ are the ramp-up and ramp-down limits of unit k. T_k denotes that active output power of kth thermal generator at time t.

In the multi-period model, the charging/discharging power is scheduled simultaneously, which follows the relationship

$$E_n^t = P_{DCH,n}^t - P_{CH,n}^t \qquad \forall t \in \Omega_T \tag{21}$$

where $P_{CH,n}^t$ and $P_{DCH,n}^t$ are the nth aggregator's charging power and V2G power of time period t. And the total V2G power E_n^t equals to the V2G power minus the charging power.

The PEV charging/discharging power are constrained in (21), which indicates the total charging demand should be met and the total charged energy does not exceed EV's capacity:

$$\sum_{m\in\Gamma_{n,t_\varepsilon}} \beta_{n,m}(S_{\text{MAX},n,m} - S_{Init,n,m}) \geq \sum_{t=1}^{t_\varepsilon}(-E_n^t)\Delta t \geq \sum_{m\in\Gamma_{n,t_\varepsilon}} \beta_{n,m}(S_{EXP,n,m} - S_{Init,n,m}) \qquad \forall t_\varepsilon \in \Omega_T \tag{22}$$

where Δt is the length of each time period and is set to 1 hour in this paper. $\beta_{n,m}$ is the battery capacity of the mth PEV affiliated to the nth aggregator. Γ_{n,t_ε} is the set of the nth EV aggregator's PEVs that should be charged to the expected level for departure by the end of time interval t_ε. $S_{\text{MAX},n,m}$ is the capacity of the mth PEV affiliated to the kth EV aggregator. $S_{EXP,n,m}$ is the expected

value of state of charge (SOC) when the mth PEV affiliated to the kth EV aggregator plugs out the grid. $S_{Init,n,m}$ is the initial value of state of charge (SOC) when the mth PEV affiliated to the kth EV aggregator in out the grid.

3) *Modifications of the Origin Constraints to the Multiple Periods:*

The constraints (14) – (18) should be satisfied in each period of the multi-objective optimization, which are stated as follows:

$$(14)-(18) \qquad \forall\ t \in \Omega_T$$

$$E_n^{\min,t} \leq E_n^t \leq E_n^{\max,t} \qquad \forall t \in \Omega_T \tag{23}$$

$$0 \leq P_{CH,n}^t \leq P_{CH,n}^{\max,t} \qquad \forall t \in \Omega_T \tag{24}$$

$$0 \leq P_{DCH,n}^t \leq P_{DCH,n}^{\max,t} \qquad \forall t \in \Omega_T \tag{25}$$

Where (23) – (25) indicate the total V2G power, charging power and V2G power of time period t should follow their upper and lower limits.

IV. MULTIPLE GROUP SEARCH OPTIMIZATION BASED ON DECOMPOSITION

A. General Framework

The proposed MOOP is very hard to solve and easily trapped by local optima due to its complicated nonconvex and nonlinear nature. To overcome this obstacle, a novel MGSO/D method, which combines 2 powerful optimization tools, is applied in this work. Firstly, decomposition strategy is used to divide the MOOP into a few subproblems to optimize simultaneously and reduce the computational complexity [25]. Secondly, the producer-scrounger model is innovatively incorporated as the main population generation methodology [23] in each subproblem to enhance the population diversity. Under this mechanism, the population is no longer evaluated iteratively like GSO, thus the efficiency of the proposed method is improved. To the best of authors' knowledge, it is the first time to employ the combination of advantages of decomposition and producer-scrounger mechanism to solve the proposed MOOP considering PEVs and wind power uncertainties.

B. Decomposition of the Proposed Multi-objective Optimization Problem

The Tchebycheff approach [25] is employed to decompose the MOOP with N^{OBJ} objectives into C scalar optimization subproblems by adjusting the jth subproblem's weight vector $\boldsymbol{\lambda}^j = (\lambda_1^j,...,\lambda_{N^{\mathrm{OBJ}}}^j)^{\mathrm{T}}$, and the objective function of the jth subproblem is

$$\min \quad g^{te}(\mathbf{x}\,|\,\boldsymbol{\lambda}^j,\mathbf{z}) = \max_{1 \leq i \leq N^{\mathrm{OBJ}}} \left\{ \lambda_i^j\,|\,f_i(\mathbf{x}) - z_i\,| \right\} \qquad \mathbf{x} \in \Omega \tag{26}$$

where Ω is the decision (variable) space. $\mathbf{z} = (z_1,...,z_{N^{\mathrm{OBJ}}})^{\mathrm{T}}$ is the reference point vector and z_i is to store the best ith single objective fitness value for each $i=1, ..., N^{\mathrm{OBJ}}$. At each run, MGSO/D will minimize all these C subproblems simultaneously, and

the best solutions obtained so far for every subproblem constitute the population. The *j*th subproblem is optimized by using only the current solutions of its neighborhood subproblems because it is believed that the neighboring subproblems' optimal solutions should be close to each other and be helpful for the optimization.

C. Innovatively Incorporated Producer-Scrounger Model

Producer-scrounger model of GSO is an efficient framework inspired by the animal searching behavior. It is innovatively incorporated in the proposed algorithm for its merit of providing diverse and well-scattered population, which contributes to the resulted PF's performance. The population of the GSO is defined as a *group*, and individuals in the population are defined as *members*. GSO group consists of *producers* for resource searching, *scroungers* for joining resources uncovered by others, and *rangers* for performing random walks to avoid local optimum [23]. If the optimal solution is in an *N*-dimensional search space, each member has a current position $\mathbf{x} \in \mathbb{R}^N$ and a head angle $\mathbf{\phi} = (\varphi_1, \ldots, \varphi_{N-1}) \in \mathbb{R}^{N-1}$. The search direction of each member is a unit vector $\mathbf{D}(\mathbf{\phi}) = (d_1, \ldots, d_N) \in \mathbb{R}^N$, which can be solved from $\mathbf{\phi}$ by a polar to Cartesian coordinate transformation [32]:

$$d_1 = \prod_{q=1}^{N-1} \cos(\varphi_q) \tag{27}$$

$$d_j = \sin(\varphi_{j-1}) \cdot \prod_{q=j}^{N-1} \cos(\varphi_q) \quad (j = 2, \ldots, N-1) \tag{28}$$

$$d_N = \sin(\varphi_{N-1}) \tag{29}$$

One subproblem and its *Y*-1 selected neighbor subproblem combines a searching group, and *Y* swarm members of each searching group are categorized into producers, scroungers and rangers to carry out different searching strategies:

1) *Producer*: The producer uses the food searching mechanism inspired from animals to find new optimal results. The member with the best single objective fitness is designated to be the producer. The solution of the chosen objective has the greatest orders of magnitude among all objectives. The producer will scan the vision field, which is distinguished by the current position $\mathbf{x}_p$, maximum pursuit angle $\theta_{\max} \in \mathbb{R}^1$, and maximum pursuit distance $l_{\max} \in \mathbb{R}^1$, by randomly sampling 3 points [23]:

a point at zero degree:

$$\mathbf{x}_z = \mathbf{x}_p + r_1 l_{\max} \mathbf{D}_p(\mathbf{\phi}) \tag{30}$$

a point in the left-hand side hypercube:

$$\mathbf{x}_l = \mathbf{x}_p + r_1 l_{\max} \mathbf{D}_p(\mathbf{\phi} - \mathbf{r}_2 \theta_{\max} / 2) \tag{31}$$

and a point in the right-hand side hypercube:

$$\mathbf{x}_r = \mathbf{x}_p + r_1 l_{\max} \mathbf{D}_p(\mathbf{\phi} + \mathbf{r}_2 \theta_{\max} / 2) \tag{32}$$

where $r_1 \in \mathbb{R}^1$ represents a normal distributed random number with average 0 and standard deviation 1; $\mathbf{r}_2 \in \mathbb{R}^{N-1}$ denotes a uniformly distributed random sequence in the range (0,1).

The producer tries to search the best point, and if there is a point in these 3 points with better resource (better fitness value) than the current position, the producer will move to the point. If not, it will not change its position and update its head to a new angle φ^{new}:

$$\boldsymbol{\varphi}^{new} = \boldsymbol{\varphi} + \mathbf{r}_2 \alpha_{\max} \tag{33}$$

where $\alpha_{\max} \in \mathbb{R}^1$ is the maximum turning angle.

2) *Scroungers*: Part of group members are chosen as scroungers to join the resources found by the producer, whose behavior is to move across for searching in the immediate area around the producer. This behavior of random walking toward the producer could be expressed as:

$$\mathbf{x}^{new} = \mathbf{x} + \mathbf{r}_3 \circ (\mathbf{x}_p - \mathbf{x}) \tag{34}$$

where $\mathbf{x}^{new}$ is the new position; $\mathbf{r}_3 \in \mathbb{R}^N$ is a uniform random vector in the range (0, 1); Operator "$\circ$" figures the entry-wise product of 2 matrices. During this scrounging, the scrounger will go on searching for other chances to join [23], and the scrounger's head angle is updated by Eq. (33).

3) *Rangers*: Other group members are rangers, which employ random walks to perform efficient searching that starts without cues leading to randomly distributed resources and benefits the population diversity. Ranger's head angle is updated in the similar way of Eq. (33) but the $\alpha_{\max}$ is set to be 2π to improve its searching ability:

$$\boldsymbol{\varphi}^{new} = \boldsymbol{\varphi} + 2\pi \mathbf{r}_4 \tag{35}$$

where $\mathbf{r}_4 \in \mathbb{R}^{N-1}$ represents a uniform distributed random sequence in the range (0,1), and then the ranger selects a random distance $a \cdot l_{\max}$ and moves to the new position:

$$\mathbf{x}^{new} = \mathbf{x} + a \cdot r_5 l_{\max} \mathbf{D}(\boldsymbol{\varphi}^{new}) \tag{36}$$

where $r_5 \in \mathbb{R}^1$ denotes a normal distributed random number with mean 0 and standard deviation 1 and $a \in \mathbb{R}^1$ is a constant.

D. Solving Process

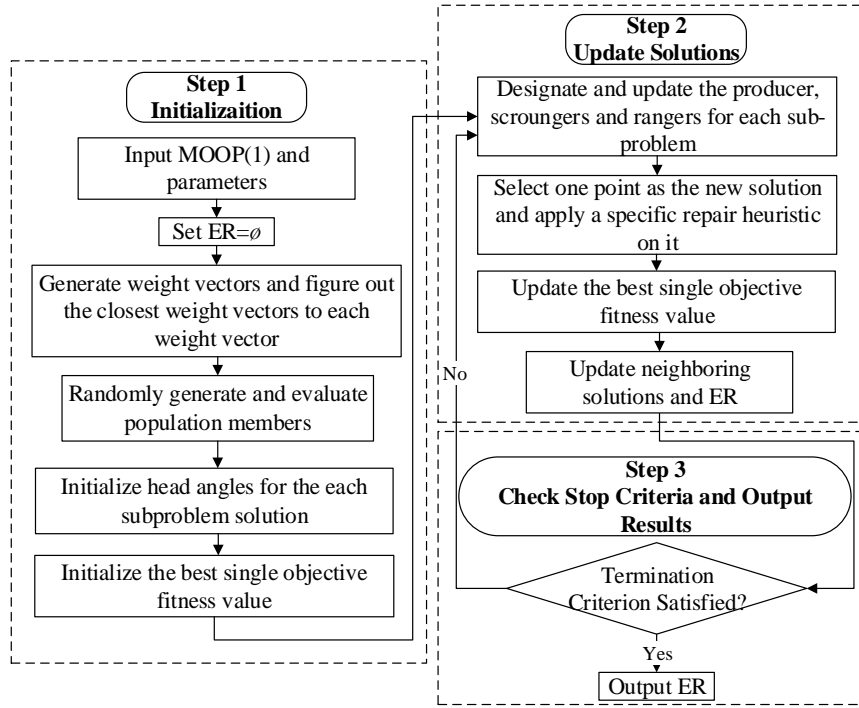The major steps of the framework are demonstrated below and depicted in Fig.1.

12

Fig.1. Flowchart of MGSO/D to solve the proposed problem

Step 1) Initialization

Step 1.1) Set ER= $\emptyset$, where ER is the external repository [25] to preserve the nondominated solutions found during the search process.

Step 1.2) Generate C evenly spread weight vectors $\boldsymbol{\lambda}^1$, …, $\boldsymbol{\lambda}^C$ related to the C subproblems respectively.

Step 1.3) Calculate the *Euclidean* distance between any 2 weight vectors and then find the B nearest weight vectors of each weight vector. For each j=1, …, C, define its neighborhood set to be $NE(j)=\{j_1, …, j_B\}$, where $\{\boldsymbol{\lambda}^{j_1},...,\boldsymbol{\lambda}^{j_B}\}$ are the B nearest weight vectors of $\boldsymbol{\lambda}^j$.

Step 1.4) Randomly generate an initial population $\mathbf{x}^1$, …, $\mathbf{x}^C$. For the jth subproblem, calculate its fitness function value vector $\mathbf{FV}^j=F(\mathbf{x}^j)$. Randomly initialize head angles $\boldsymbol{\varphi}$ for the solution of each subproblem. Initialize $\mathbf{z}$ randomly.

Step 2) Updating subproblem solutions

For j=1, …, C, perform steps as follows:

Step 2.1) Reproduction:

(1) Producer Designate the best individual in B group members as the producer $x^w(\varphi^w)$ with the index w.

(2) Producing The producer makes producing by (30)-(33).

(3) Scrounging Except the producer, randomly choose [80% (Y-1)] members from B-1 group members as scroungers and carry out scrounging using (33)-(34).

(4) Ranging Except the producer and scroungers, other members are rangers and carry out ranging using (35)-(36).

13

Then randomly select one point from the Y points as the new solution **y**.

    Step 2.2) **Improvement**: apply the greedy repair producer [37] on **y** to produce **y'** to eliminate the infeasible solutions and improve the efficiency of the solving process.

    Step 2.3) **The updating of z**: for every $i=1, …, N^{OBJ}$, when $z_i > f_i(\mathbf{y}')$, set $z_i = f_i(\mathbf{y}')$.

    Step 2.4) **The updating of Neighboring Solutions**: For every index $i \in NE(j)$, if $g^{te}(\mathbf{y}' / \boldsymbol{\lambda}^i, \mathbf{z}) \leq g^{te}(\mathbf{x}^i / \boldsymbol{\lambda}^i, \mathbf{z})$, set $\mathbf{x}^i = \mathbf{y}'$ and $FV^i = F(\mathbf{y}')$.

    Step 2.5) **The updating of ER:** Omit all the vectors dominated by $F(\mathbf{y}')$ from ER, and add $F(\mathbf{y}')$ to ER otherwise.

Step 3) Termination

If the stopping criteria is met, terminate and export ER. If not, go back to **Step 2)**.

E. Performance Metrics of the Proposed Multiple Group Search Optimization Based on Decomposition Method

It is hoped that the obtained PF by the MGSO/D could be close enough to the true PF. However, the true PF is very hard to find and guarantee, and the reference PF [34] is used instead. Here the PF solutions obtained by the NSGA-II [33], MGSO [24], MOEA/D [25] and MGSO/D are ranked by dominance comparisons to select the reference PF. Afterwards, 4 indices are utilized to compare the PF solution quality of MGSO/D with other typical algorithms. 1) *Convergence metric*: measuring the closeness degree from the reference PF to the obtained PF. For each obtained PF, the minimum Euclidean distance between each solution on the obtained PF and solutions on the reference PF is computed, and the mean of these distances is defined as the convergence metric [33]. 2) *Span metric*: measuring the normalized Euclidean distance of the boundary solutions [35] for MOOP objectives, which estimates the spread of the PFs. 3) *Spacing metric* [36]: calculating the relative crowding distance between adjacent solutions on the obtained PF. This metric is adopted to evaluate the distribution uniformity of the resulting PF. 4) l_{max}/l_{min} *metric* [39]: It is the ratio of maximum distance of consecutive Pareto points to the minimum distance, which is an indicator to measure the spatial distribution of PF solutions and can be the supplement of the spacing metric.

V.   Numerical Results and Analysis

A. Investigation on the Modified IEEE 30-Bus System

A modified IEEE 30-bus system is considered to evaluate the proposed model and algorithm for dual-objective dispatch. The topology and parameters including the thermal generation cost and emission coefficients can be found in [38]. 2 wind farms are located on node 10 and 15, while 2 PEV aggregators are located on node 3 and 18. Their relevant information is respectively depicted as follows [17][29]: For wind farm generators, $\gamma_1 = \gamma = 2$, $\gamma_2 = 2\gamma$, $h_1 = h = 5$, $h_2 = 2h$, $l = 2$, $v_m = 5$m/s, $g_m^W = 10\$/MWh$, $\varepsilon_m^{W,p} = 30\$/MWh$, $\varepsilon_m^{W,r} = 70\$/MWh$; for PEV aggregators, $r = 0.2$, $C^{BI}/E^B = 100\$/kWh$, $L^C = 1000$, $d^{DOD} = 0.8$, $\mu = 1$, $\phi = 6$, $g_n^E = 65\$/MWh$, $\varepsilon_n^{E,p} = 30\$/MWh$, $\varepsilon_n^{E,r} = 70\$/MWh$. For fair comparisons, the maximum numbers of generations in 4 benchmarks are equal to 200.

To determine the optimum settings for each algorithm, 20 independent runs of each algorithm are carried out. The key settings for the algorithm are: $Y=3$, $C=33$, $B=20$.

1) *Case 1*: A dual-objective problem is studied to optimize the generation cost f_1 and emission f_2 in this case. The averages of 4 performance metrics on convergence, span, l_{max}/l_{min} and spacing measures over the 20 optimization runs for different algorithms are tabulated in row 2-5 of Table I. In this case, the reference PF used for computing the convergence metric consists of 257 nondominated solutions, in which 48.63% and 51.37% of the solutions are offered by MOEA/D and MGSO/D. It reveals that all of the solutions found by NSGA-II and MGSO are dominated by those obtained by MOEA/D and MGSO/D, and MGSO/D has contributed more to form the reference PF solutions than MOEA/D. It can also be observed that the solutions obtained by the proposed algorithm are closer to the true PF.

It could be pointed out from row 2-5 of Table I that the convergence metric of the proposed algorithm is much lower than those of other benchmarks, which means MGSO/D can most effectively obtain the non-dominated solutions in the separated feasible islands. Besides, the maximum normalized span indicates MGSO/D has a more powerful global exploratory capability than other algorithms. Furthermore, the proposed algorithm performs best in the l_{max}/l_{min} and spacing metric, and it illustrates that the PF outlines of proposed algorithm are more uniformly-distributed. Therefore, it can be concluded the proposed algorithm can markedly outperform other 3 methods, and provides satisfactory performance on these 4 indices.

TABLE I

RESULTING STATISTICS OF PERFORMANCE METRICS IN CASE 1-3

Case	Metrics	NSGA-II	MGSO	MOEA/D	MGSO/D
Case 1	convergence	0.040145	0.047759	0.017542	**0.013515**
	span metric	0.457428	0.913644	1.052471	**1.309735**
	l_{max}/l_{min}	64.20240	58.00052	10.31539	**7.460752**
	spacing metric	0.106931	0.219106	0.018393	**0.017782**
Case 2	convergence	0.121255	0.034027	0.007484	**0.005917**
	span metric	0.818879	1.079506	1.094476	**1.226634**
	l_{max}/l_{min}	74.29048	63.58833	18.93584	**14.30798**
	spacing metric	0.201233	0.261979	0.037620	**0.036508**
Case 3	convergence	0.123154	0.104922	0.011829	**0.011321**
	span metric	0.739562	0.736552	1.228029	**1.409085**
	l_{max}/l_{min}	68.48074	106.59971	20.16012	**15.92876**
	spacing metric	0.182097	0.171581	**0.031338**	0.033932

Table II listed the best solutions for emission and generation cost obtained by the boundary solutions in the PFs of the best runs of all algorithms and the corresponding PF solutions are plotted in Fig. 2. The results indicate that the best run of

MGSO/D achieves outstanding diversity with 2 better boundary solutions compared with other 3 algorithms. Meanwhile, the best PF with MGSO/D could find solutions with much better fitness on the objectives of the generation cost and the emission compared to other 3 algorithms. The decomposition approach helps MGSO/D have higher exploratory capability than MGSO. Meanwhile, the producer-scrounger model also enhances its searching ability than MOEA/D.

TABLE II

COMPARISON OF BEST SOLUTIONS IN CASE 1

Case 1	Best generation cost				Best emission			
	A	B	C	D	A	B	C	D
f_1	590.26	623.65	538.81	**521.55**	831.93	895.72	877.48	897.52
f_2	0.2360	0.2273	0.2448	0.2468	0.2001	0.1962	0.1962	**0.1956**

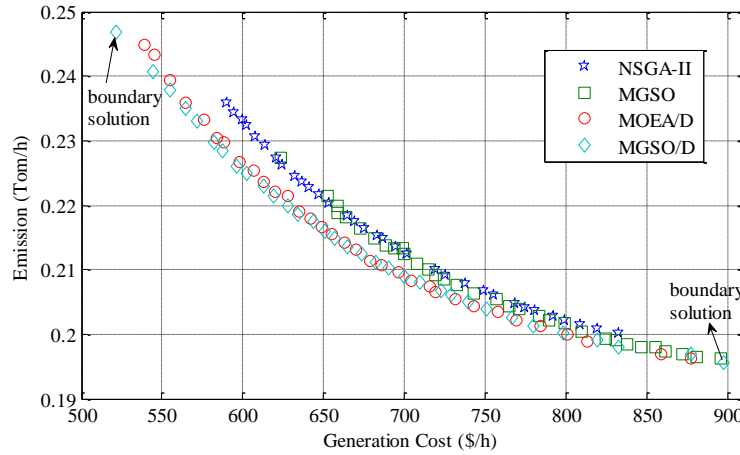**A: NSGA-II; B: MGSO; C: MOEA/D; D: MGSO/D; f: fitness value**

Fig. 2. The best PFs obtained for Case 1.

2) *Case 2-3*: Further, overall performances of 4 benchmarks to solve Case 2-3 dual-objective MOOPs are also listed in Table I. In Case 2, the MOOP has 2 competing objectives of the emission f_2 and power loss f_3 while the objectives in Case 3 are the generation cost f_1 and power loss f_3. In Case 2, MGSO/D again performs well on convergence, span, l_{max}/l_{min} and spacing metrics. Besides, MGSO/D performs the best in the metrics of convergence, span and l_{max}/l_{min} in Case 3. Although the PFs of MOEA/D have slightly smaller spacing metric than MGSO/D, which means PF points from MOEA/D are more uniformly-spaced only by a very small margin, MOEA/D performs worse in other 3 metrics.

Case 1-3 confirm that, for these 3 different dual-objective problems, the proposed MGSO/D algorithm can effectively propagate the search to obtain the uniformly distributed and diverse PF, and have a relatively better performance than NSGA-II, MGSO and MOEA/D.

3) *Uncertainty Discussion*: To investigate the uncertainties of V2G and wind power, the impacts of PDF parameters of h and ϕ in Case 3 are studied. At the same power loss level, it could be observed in Fig. 3 that the generation cost increases when the

16

standard deviation ϕ of V2G PDF grows. Table III shows that the impact of ϕ on best solutions for power loss and generation cost obtained by the boundary solutions in the PFs of the best runs in Case 3. It can be seen that when ϕ equals 6, boundary solutions are better than those with other ϕ which are larger than 6. Table V gives the quantified impact of uncertainty of V2G power on Pareto optimization results in Case 3, which tabulates the performance metrics on convergence, span, l_{max}/l_{min} and spacing measures over the 20 optimization runs when the values of ϕ are 6, 8, 10 and 12. And the results confirm that the V2G power uncertainty influences the Pareto solutions significantly, especially on the convergence and span metrics. The convergence metric of the proposed algorithm becomes larger when the value of ϕ grows, which indicates the uncertainty of V2G weakens the algorithm's ability to obtain the non-dominated solutions in the separated feasible islands. Besides, it can be noted the span metric of Pareto front decreases when the standard deviation ϕ of V2G PDF increases, which indicates he powerful global exploratory capability can be enhanced if the uncertainty of V2G power is reduced.

Different values of wind power PDF h will also lead to different Pareto curves as shown in Fig. 4. Generally, at the same generation cost level, power loss becomes smaller when the parameter h gets larger. Table IV shows that when h equals 18, least power loss is obtained, and when h equals 20, least generation cost is obtained. Table VI demonstrates the quantified result statistics of performance metrics for different uncertainty parameter h of wind power over 20 optimization runs in Case 3. It can be found that the metric of convergence decreases with the increasing of the h values, and the quantified resulting statistics shows that the uncertainties of wind speed clearly affects the convergence performance of the Pareto optimization. These results clearly indicate the uncertainties significantly influences the Pareto solutions of the optimization. Therefore, it is important to account the uncertainties during the power system dispatch for better utilization of the V2G and wind power.

Obviously, the parameters in the mathematical model should be adjusted to minimize the impact of uncertainty on Pareto solutions. It can be concluded that reducing the standard deviation of V2G power ϕ will lead to a better performance of Pareto optimization and minimize the impact of uncertainty. Although the behaviors of EVs are usually stochastic and unpredictable, the charging and discharging of EVs are still partly controllable, thus there are several manners to adjust this parameter and decrease the impacts of V2G uncertainties. For example, establishment of information exchange mechanism between EVs and dispatch center could provide more information such as plug-in and plug-out time, or SOCs, and reduce the uncertainties of Pareto optimization. Meanwhile, some financial incentives such as V2G price subsidies will encourage information sharing and reduce uncertainties. However, for the uncertainties of wind power, the parameters of the scale factor h or sharp factor γ at a given location cannot be adjusted because they are directly related to the natures of wind speed, which are uncontrollable. For the dispatchers, they can still adjust the coefficients of underestimated penalty and overestimated penalty cost $\varepsilon_m^{W,p}$ and $\varepsilon_m^{W,r}$ to minimize the impact of uncertainties on Pareto results.

TABLE III

COMPARISON OF BEST SOLUTIONS WITH DIFFERENT UNCERTAIN PARAMETER ϕ IN CASE 3

Case 3	Best generation cost				Best power loss			
	ϕ=6	ϕ=8	ϕ=10	ϕ=12	ϕ=6	ϕ=8	ϕ=10	ϕ=12
f_1	**519.90**	603.84	700.06	785.95	841.01	862.90	978.90	1040.26
f_3	0.0794	0.0782	0.0655	0.0654	**0.0199**	0.0211	0.0201	0.0203

TABLE IV

COMPARISON OF BEST SOLUTIONS WITH DIFFERENT UNCERTAIN PARAMETER H IN CASE 3

Case 3	Best generation cost				Best power loss			
	h=10	h=15	h=18	h=20	h=10	h=15	h=18	h=20
f_1	519.90	515.81	500.18	**491.18**	841.01	789.65	800.44	813.22
f_3	0.0794	0.0719	0.0759	0.0839	0.0199	0.0206	**0.0199**	0.0210

TABLE V

RESULTING STATISTICS OF PERFORMANCE METRICS FOR DIFFERENT UNCERTAIN PARAMETER ϕ OF V2G POWER IN CASE 3

ϕ	Span	l_{max}/l_{min}	Spacing	Convergence
6	**1.1750829**	15.56302392	0.0287306	**0.00152921**
8	**1.0814451**	14.16955953	0.0216976	**0.127101822**
10	**0.9331446**	9.479548093	0.0150633	**0.208092719**
12	**0.9028379**	12.92415393	0.0208708	**0.297852799**

TABLE VI

RESULTING STATISTICS OF PERFORMANCE METRICS FOR DIFFERENT UNCERTAIN PARAMETER H OF WIND POWER IN CASE 3

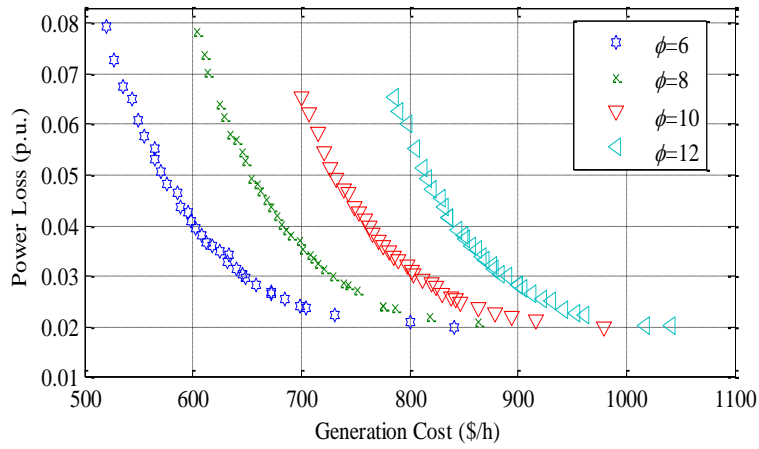| h	Span	l_{max}/l_{min}	Spacing	Convergence
10	1.3062154	24.75712786	0.0352925	**0.044937927**
15	1.1200759	38.98411999	0.0175459	**0.018124251**
18	1.2252446	313.6315745	0.0199739	**0.003573183**
20	1.3465841	32.44088639	0.0276637	**0.003159928**

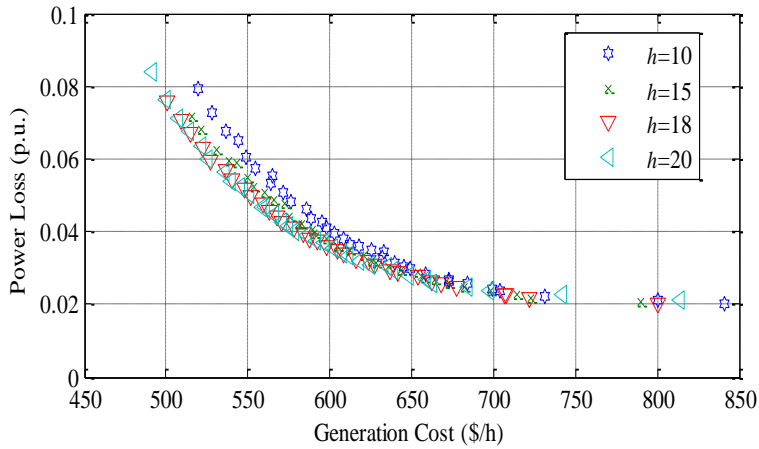Fig. 3. PFs for different uncertain parameter ϕ of V2G power in Case 3.

Fig. 4. PFs for different uncertain parameter h of wind power in Case 3.

B. Investigation on the Modified IEEE 118-Bus System

Case 4: To investigate the performance of MGSO/D on large-scale power systems, a modified 118-bus system [40] consisting of 54 generators and 186 branches is used for a 3-objective optimization to reduce generation cost, emission and power loss. 6 wind farms are installed on node 11, 23, 45, 60, 82 and 106. In addition, 5 PEV aggregators are located on node 2, 18, 44, 75 and 102. The parameters of wind farms and PEV aggregators are the same with the former cases. To make it a fair comparison, the size of the PFs and the iteration number of each algorithm are all set to 45 and 200, respectively. The settings for MGSO/D are: Y=3, C=45, B=15. For MOEA/D, subproblem number is equal to 45 the same as MGSO/D. Additionally, M_p of MGSO and the population size of NSGA-II are set to 283 and 855, respectively to make their number of function evaluations be equal to MGSO/D. 20 independent runs of all comparative algorithms are carried out.

The reference PF for computing the convergence reference consists of 135 solutions, 38.52% of which (52 solutions) is obtained by MOEA/D and the rest of the reference PF containing 83 points is found with MGSO/D. It can be observed that all solutions obtained from NSGA-II and MGSO are covered by those of MOEA/D and MGSO/D. It again confirms the great ability of MGSO/D to obtain a set of solutions closer to the true Pareto set and its high potential to find Pareto optimality.

19

Furthermore, the resulting statistics of performance metrics of each algorithm are shown in Table VII, which demonstrate that, MGSO/D markedly outperforms the other 3 benchmarks, on the convergence, span, l_{max}/l_{min} and spacing metrics. These statistical comparative experiments indicate that MGSO/D has the superior ability and efficiency of solution searching to guarantee the quality of PF solutions when the proposed algorithm deals with high dimensional MOOP with complex and nonlinear power system constraints. Moreover, the variances of the convergence, l_{max}/l_{min} and spacing metrics confirm the stable performance of MGSO/D for the resulting Pareto set on these 3 measures. Although the variance of span metric of MGSO/D is not the best in 4 algorithms, its worst span metric in 20 runs is much higher than other benchmarks. Overall, in dealing with large-scale MOOP, the proposed algorithm also shows its obvious advantages.

TABLE VII

RESULTING STATISTICS OF PERFORMANCE METRICS IN CASE 4

Case 4		Best	Worst	Average	Variance
convergence	NSGA-II	0.390974	0.840298	0.596639	0.008647
	MGSO	0.154348	0.337800	0.232941	0.003117
	MOEA/D	0.010663	0.103243	0.044616	0.000523
	MGSO/D	**0.009850**	**0.065725**	**0.037132**	**0.000290**
span metric	NSGA-II	0.021917	0.000426	0.010284	4.43E-05
	MGSO	0.021253	0.003820	0.013042	**2.01E-05**
	MOEA/D	0.028060	0.003516	0.013738	4.33E-05
	MGSO/D	**0.064891**	**0.006659**	**0.016972**	1.67E-04
l_{max}/l_{min}	NSGA-II	22.25166	124.6999	79.97006	1105.110
	MGSO	38.10994	159.1815	87.44264	1382.437
	MOEA/D	22.39172	239.2425	54.84145	2574.360
	MGSO/D	**20.78305**	**77.25710**	**38.17302**	**193.5422**
spacing metric	NSGA-II	0.000601	0.009117	0.005002	5.46E-06
	MGSO	0.008498	0.077129	0.026255	3.62E-04
	MOEA/D	0.001383	0.087310	0.007464	3.37E-04
	MGSO/D	**0.001367**	**0.003574**	**0.002302**	**3.69E-07**

In addition, the best run of each algorithm is plotted in Fig. 5. It is obviously that MGSO/D shows significant superiority in the searching ability than the other algorithms, especially NSGA-II and MGSO. It can also be observed that the proposed algorithm is able to obtain solutions with superior fitness on 3 objectives compared with other 3 benchmarks.

Because the calculation time is also an important indicator to measure the advantage of an algorithm, the solution time of different algorithms in different scenarios is compared and analyzed in Case 4. Load level is a major uncertainty which affects the power generation, emission and power loss significantly. Therefore, three typical scenarios are constructed according to

different load levels in this case. Scenario 1: the load level is set to be 100% $\times$ predicted load level; Scenario 2: the load level is set to be 90% $\times$ predicted load level; Scenario 3: the load level is set to be 110% $\times$ predicted load level.
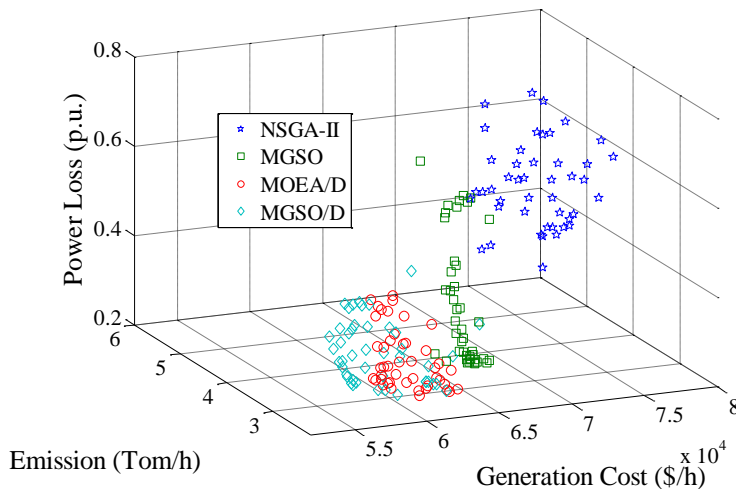

Fig. 5. The best PFs obtained for Case 4.

The solution time of different algorithms in 3 scenarios are demonstrated in Table VIII. It can be seen that in Case 4, for the 3-objective optimization problem, the computation time of MGSO/D is less than NSGA-II and MGSO, but longer than MOEA/D. Therefore, the calculation speed of MGSO/D is not the best in solving mentioned optimization problems. However, the Pareto front obtained by the proposed algorithm is of better quality than those obtained by other algorithms. It would be an acceptable small compromise to sacrifice the solution time slightly to trade for the high-quality Pareto front using MGSO/D. It can also be found that the solution time of different algorithms would vary slightly in different scenarios but remains comparable.

TABLE VIII

THE SOLVING TIME OF DIFFERENT ALGORITHMS IN DIFFERENT SCENARIOS IN CASE 4

Solving time (s)		NSGA-II	MGSO	MOEA/D	**MGSO/D**
Case 4	Scenario 1	96.088	65.669	9.146	**64.106**
	Scenario 2	98.188	63.538	9.243	**63.381**
	Scenario 3	105.09	69.323	9.676	**62.867**

C. *Group Member Number Effects on the Performance of the Multiple Group Search Optimization Based on Decomposition Method*

Case 5: Group member number (Y) is a crucial parameter influencing the searching ability of MGSO/D. To investigate the effect of Y on the performance of MGSO/D, PFs are obtained as Y is 3, 10, 15 or 20 when a dual-objective MOOP with the objectives of the generation cost and emission is studied in the modified IEEE 30-bus system in Case 5. For each Y, 10 independent runs

were carried out in this case. Resulting statistics of performance metrics for Y=3, 10, 15 and 20 are detailed in Table IX.

Although the spacing metric of Y=3 is a little worse, it can be observed the proposed algorithm performs better when Y=3 on

convergence metric, span metric and l_{max}/l_{min} than those of Y=10, 15 and 20, which demonstrates the best searching ability is

obtained when Y=3. As shown in Fig. 6, the PFs of the best runs for Y=3, 10, 15 and 20 are compared. It can be found that

MGSO/D (Y=3) can find solutions with better fitness values (emission and generation cost) than those when Y= 10, 15 and 20. It

is also noted that the PFs of the best run for Y=3 performs better with outstanding diversity and spanning.

TABLE IX

RESULTING STATISTICS OF PERFORMANCE METRICS IN CASE 5

| Case 5	Y	Best	Worst	Average	Variance
convergence	3	**0.002881**	**0.010480**	**0.005994**	4.453E-06
	10	0.004331	0.024719	0.014579	3.625E-05
	15	0.005165	0.015557	0.008953	1.436E-05
	20	0.009089	0.016087	0.010991	**3.932E-06**
span metric	3	**1.423644**	**1.346044**	**1.397212**	**0.000473**
	10	1.044234	0.761052	0.904963	0.007660
	15	1.041209	0.668055	0.826955	0.010460
	20	0.883343	0.583129	0.762124	0.009282
l_{max}/l_{min}	3	**3.628087**	**8.392825**	**6.168374**	**2.379713**
	10	4.867813	14.807929	7.503204	7.247219
	15	4.164266	18.941727	8.481762	17.62801
	20	4.261702	11.807636	7.892960	6.100200
spacing metric	3	0.011898	0.024077	0.017328	1.663E-05
	10	0.011286	0.020898	0.016840	**1.013E-05**
	15	0.006316	0.020880	0.015017	1.825E-05
	20	**0.007743**	**0.016995**	**0.011220**	1.141E-05
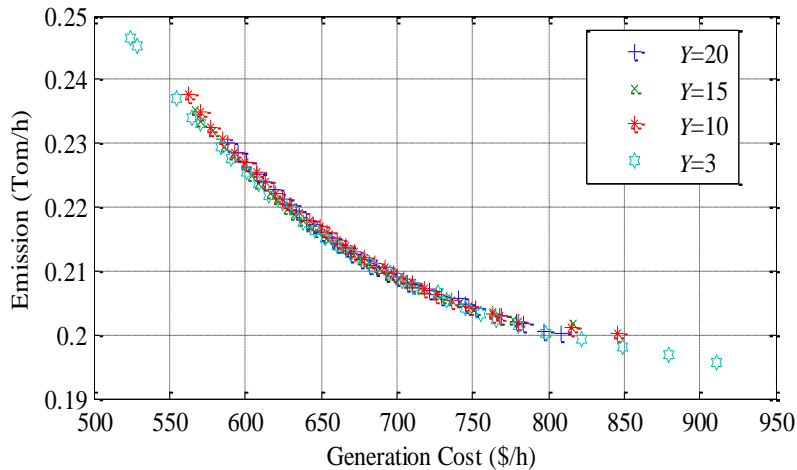
Fig. 6. Comparison of the PFs of the best runs for *Y*=3, 10 and 20

D. *Case 6: Results of the Multi-period Multi-objective Optimal Dispatch Model*

In Case 6, a multi-period dual-objective optimal dispatch model with the objectives of the generation cost and emission in the modified IEEE 30-bus system is solved by MGSO/D. Pareto solutions are obtained as shown in Fig.7. One of these non-dominated solutions as pointed out in Fig. 7 is selected to show in details in Figs. 8-10. Fig. 8 illustrates the output of the V2G power on node 18 for 24 hours. When the value of V2G power is negative, it means the charging cycles for EVs. It can be seen from Fig. 8 that the PEV aggregator on node 18 does not always serve as V2G power (i.e. at 1:00 am and 10:00 pm) but plays a role as load in most time of a day (i.e. at 3:00 am and 5:00 pm). It is because the expected value of SOC of PEV when PEV plugs out the grid should be satisfied. As shown in Fig. 8, the charge and discharge characteristics in different periods of a day are well considered in the multi-period multi-objective optimal dispatch model.
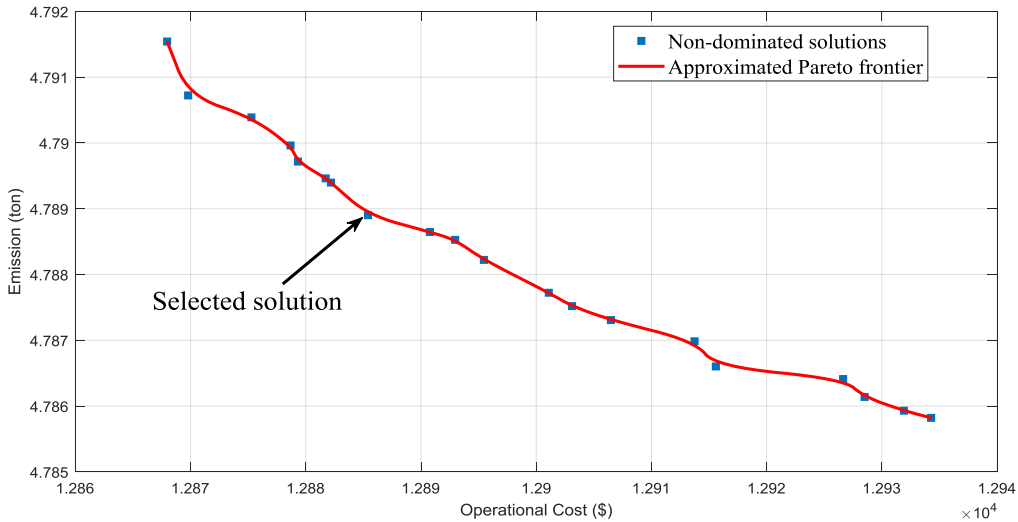
Fig. 7 Pareto solutions for the multi-period multi-objective optimal dispatch model

23
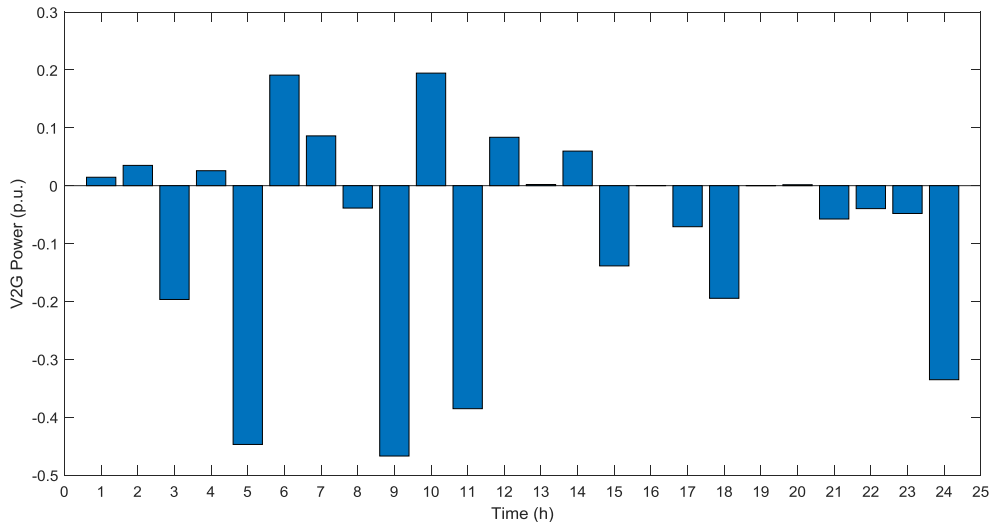
Fig. 8 Output of the V2G Power in the multi-period multi-objective optimal dispatch model

Fig. 9 and Fig. 10 compare the output of thermal generator on node 8 in the multi-period multi-objective optimal dispatch model with and without consideration of ramp rate constraints of thermal generators. Thermal generator outputs on node 8 during time period 13 and time period 14 are marked by red dotted lines to illustrate the effectiveness of ramp rate constraints. Fig. 10 shows that the outputs of the thermal generator on node 8 at 13:00 pm and 14:00 pm are apparently different and are on a sharply declining trend, which is a big challenge to ramp capacity of the generator and the reliable and secure operation of the power system. After taking into the ramp rate constraints, the decline rate decreases significantly as shown in Fig. 9. It can be concluded that considering ramp rate constraints in the multi-period dual-objective optimal dispatch model is necessary.
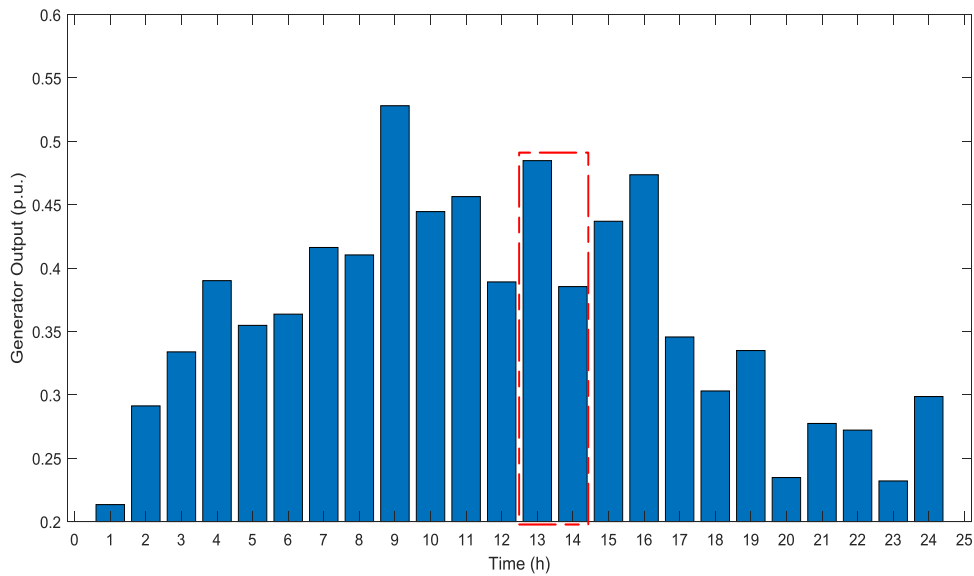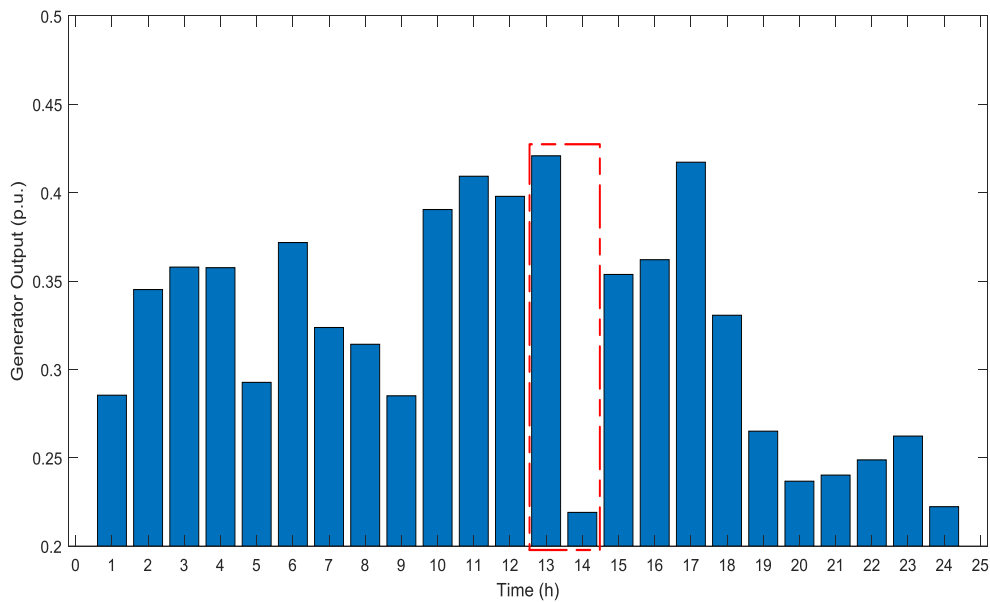

Fig. 9 Output of the thermal generator in the multi-period multi-objective optimal dispatch model considering ramp rate constraints

24

Fig. 10 Output of the thermal generators in the multi-period multi-objective optimal dispatch model without considering ramp rate constraints

VI. Conclusions

An efficient a multiple group search optimization based on decomposition algorithm, which combines the merits of decomposition strategy and producer-scrounger model, is proposed to solve a highly nonlinear constrained multi-objective optimization problem with the uncertainty of plug-in electric vehicles and wind power being considered. It has been verified that the concerned uncertainties would have significant impacts to the simulation results, and the proposed multiple group search optimization based on decomposition algorithm has superior solution searching ability in both small-size and high-dimensional multi-objective optimization problems with complex constraints and objectives, which makes it a promising framework for widely applications in solving other similar problems. Meanwhile, considering the complexity of uncertainties, it should be noted that difficulties still exist in solving the multi-objective optimization problems with uncertain factors, and the model presented in this paper is simplified to ignore the factors of EV availability, trip durations, and time of trips in the PDF of V2G power, and adopt the simpler 2-parameter distribution instead of the bivariate normal distribution in the PDF of wind power. Further research with precise modeling of these uncertain factors is an on-going work.

References

[1] W. Su, H. Tahimi-Eichi, W. Zeng, and M. Chow, "A survey on the electrification of transportation in a smart grid environment," IEEE Trans. Ind. Informat., vol. 8, no. 1, pp. 1-10, Feb. 2012.

[2] Katrin Seddig, Patrick Jochem, Wolf Fichtner, "Two-stage stochastic optimization for cost-minimal charging of electric vehicles at public charging stations with photovoltaics," Appl. Energy, Vol. 242, pp. 769-781, May 2019.

[3] Z. Darabi and M. Fedowsi, "An event-based simulation framework to examine the response of power grid to the charging demand of plug-in hybrid electric vehicles (PHEVs)," IEEE Trans. Ind. Informat., vol. 10, no. 1, pp. 313-322, Feb. 2014.

[4] L. P. Fernaìndez, T. G. S. Romaìn, R. Cossent, C. M. Domingo, and P. Friìas, "Assessment of the impact of plug-in electric vehicles on distribution networks," IEEE Trans. Power Syst., vol. 26, no. 1, pp. 206-213, Feb. 2011.

[5] K. Clement-Nyns, E. Haesen, and J. Driesen, "The impact of charging plug-in hybrid electric vehicles on a residential

distribution grid," IEEE Trans. Power Syst., vol. 26, no. 1, pp. 371-380, Feb. 2010.

[6] G. Wang, J. Zhao, F. Wen, Y. Xue and G. Ledwich, "Dispatch strategy of PHEVs to mitigate selected patterns of seasonally varying outputs from renewable generation," IEEE Trans. Smart Grid, vol. 6, no. 2, pp. 627-639, Mar. 2015.

[7] Y. Ma, T. Houghton, A. Cruden, and D. Infield, "Modeling the benefits of vehicle-to-grid technology to a power system," IEEE Trans. Power Syst., vol. 27, no. 2, pp. 1012-1020, May 2012.

[8] Chao Peng, Jianxiao Zou, Lian Lian, Liying Li, "An optimal dispatching strategy for V2G aggregator participating in supplementary frequency regulation considering EV driving demand and aggregator's benefits, " Appl. Energy, Volume 190, Pages 591-599, Mar. 2017.

[9] Y. Saber and G. K. Venayagamoorthy, "Intelligent unit commitment with vehicle-to-grid: A cost-emission optimization," J. Power Sources, vol. 195, no. 3, pp. 898-911, Feb. 2010.

[10] W. Yao, J. Zhao, F. Wen, Y. Xue and G. Ledwich, "A hierarchical decomposition approach for coordinated dispatch of plug-in electric vehicles," IEEE Trans. Power Syst., vol. 28, no. 3, pp. 2768-2778, Aug. 2013.

[11] P. Jong, A. Kiperstok, A.S. Sanchez, R. Dargaville and E.A. Torres, "Integrating large scale wind power into the electricity grid in the Northeast of Brazil", Energy, 2016, 100: 401-415.

[12] Xingxing Zhang, Marco Lovati, Ilaria Vigna, Joakim Widén, Mengjie Han, Csilla Gal, Tao Feng, "A review of urban energy systems at building cluster level incorporating renewable-energy-source (RES) envelope solutions," Appl. Energy, Volume 230, Pages 1034-1056, Nov. 2018.

[13] C. Budischak et al., "Cost-minimized combinations of wind power, solar power and electrochemical storage, powering the grid up to 99.9% of the time," J. Power Sources, vol. 225, pp. 60-74, Mar. 2013.

[14] A. Y. Saber and G. K. Venayagamoorthy, "Plug-in vehicles and renewable energy sources for cost and emission reductions," IEEE Trans. Ind. Electron., vol. 58, no. 4, pp. 1229-1238, Apr. 2011.

[15] G. Kyriakarakos, D. Piromalis, A. Dounis, and K. Arvanitis, "Intelligent demand side energy management system for autonomous polygeneration microgrids," Appl. Energy, vol. 103, pp. 39-51, Mar. 2013.

[16] P. P. Varaiya, F. F. Wu, and J. W. Bialek, "Smart operation of smart grid: Risk-limiting dispatch," Proc. IEEE, vol. 99, no. 1, pp. 40-57, Jan. 2011.

[17] J. Zhao, F. Wen, Z. Dong, Y. Xue and K. P. Wong, "Optimal dispatch of electric vehicles and wind power using enhanced particle swarm optimization," IEEE Trans. Ind. Informat., vol. 8, no. 4, pp. 889-899, Jun. 2012.

[18] T. Shekari, S. Golshannavaz and F. Aminifar, "Techno-economic collaboration of PEV fleets in energy management of microgrids," IEEE Trans. Power Syst., vol. 32, no. 5, pp. 3833-3841, Sept. 2017.

[19] G. Carpinelli, F. Mottola, D. Proto and A. Russo, "A multi-objective approach for microgrid scheduling," IEEE Trans.

Smart Grid, vol. 8, no. 5, pp. 2109-2118, Sept. 2017.

[20] T. F. Robert, A. H. King, C. S. Harry, Rughooputh, and K. Deb, "Evolutionary multi-objective environmental/economic dispatch: stochastic vs deterministic approaches", KanGAL, Rep. 2004019, 2004, pp. 1-15.

[21] M. A. Abido, "Environmental/economic power dispatch using multi-objective evolutionary algorithms," IEEE Trans. Power Syst., vol. 18, no. 4, pp. 1529–1537, Nov. 2003.

[22] M. R. Andervazh and S. Javadi, "Emission-economic dispatch of thermal power generation units in the presence of hybrid electric vehicles and correlated wind power plants," IET Gener. Transm. Distrib., vol. 11, no. 9, pp. 2232-2243, 6 22 2017.

[23] S. He, Q. H. Wu, and J. R. Saunders, "Group search optimizer: An optimization algorithm inspired by animal searching behavior," IEEE Trans. Evol. Comput., vol. 13, no. 5, pp. 973-990, Oct. 2009.

[24] B. Zhou, K.W. Chan, T. Yu and C.Y. Chung, "Equilibrium-inspired multiple group search optimization with synergistic learning for multi-objective electric power dispatch," IEEE Trans. Power Syst., vol. 28, no. 4, pp. 3534-3545, Nov. 2013.

[25] Q. Zhang and H. Li, "MOEA/D: A multi-objective evolutionary algorithm based on decomposition," IEEE Trans. Evol. Comput., vol. 11, no. 6, pp. 712–731, Dec. 2007.

[26] J. Park, K. Lee, J. Shin, and K. Y. Lee, "A particle swarm optimization for economic dispatch with nonsmooth cost functions," IEEE Trans. Power Syst., vol. 20, no. 1, pp. 34–42, Feb. 2005.

[27] S.-L. Andersson, A. K. Elofsson, M. D. Galus, L. Göransson, S. Karlsson, F. Johnsson, and G. Andersson, "Plug-in hybrid electric vehicles as regulating power providers: Case studies of Sweden and Germany," Energy Policy, vol. 38, no. 6, pp. 2751-2762, Jun. 2010.

[28] J. Tomić and W. Kempton, "Using fleets of electric-drive vehicles for grid support," J. Power Sources, vol. 168, no. 2, pp. 459-468, Jun. 2007.

[29] J. Hetzer, D. C. Yu and K. Bhattarai, "An economic dispatch model incorporating wind power," IEEE Trans. on Energy Convers., vol. 23, no. 2, pp. 603-611, Apr. 2008.

[30] V. Vahidinasab and S. Jadid, "Normal boundary intersection method for suppliers' strategic bidding in electricity markets: An environmental/economic approach," Energy Conversion and Management, vol. 51, no. 6, pp. 1111–1119, Jun. 2010.

[31] F. N. Lee, M. Lin and A. M. Breipohl, "Evaluation of the variance of production cost using a stochastic outage capacity state model," IEEE Trans. Power Syst., vol. 5, no. 4, pp. 1061-1067, Nov. 1990.

[32] D. Mustard, "Numerical integration over the n-dimensional spherical shell," Math. Comput., vol. 18, no. 88, pp. 578-589, Oct. 1964.

[33] K. Deb, A. Pratap, S. Agarwal, and T. Meyarivan, "A fast and elitist multi-objective genetic algorithm: NSGA-II," IEEE Trans. Evol. Comput., vol. 6, no. 2, pp. 182–197, Apr. 2002.

[34] C. A. Coello Coello, G. B. Lamont, and D. A. Van Veldhuizen, Evolutionary Algorithms for Solving Multi-Objective Problems. Norwell, MA, USA: Kluwer, 2002.

[35] E. Zitzler, K. Deb, and L. Thiele, "Comparison of multi-objective evolutionary algorithms: Empirical results," Evol. Comput., vol. 8, no. 2, pp. 173–195, 2000.

[36] K. Deb, Multi-Objective Optimization Using Evolutionary Algorithms. Chichester, U.K.: Wiley, 2001.

[37] A. Jaszkiewicz, "On the performance of multiple-objective genetic local search on the 0/1 knapsack problem – A comparative experiment," IEEE Trans. Evol. Comput., vol. 6, no. 4, pp. 402–412, Aug. 2002.

[38] S. Agrawal, B. K. Panigrahi and M. K. Tiwari, "Multi-objective particle swarm algorithm with fuzzy clustering for electrical power dispatch," IEEE Trans. Evol. Comput., vol. 12, no. 5, pp. 529-541, Feb. 2008.

[39] Q. Li, M. Liu and H. Liu, "Piecewise normalized normal constraint method applied to minimization of voltage deviation and active power loss in an AC–DC hybrid power system," IEEE Trans. Power Syst., vol. 30, no. 3, pp. 1243-1251, May 2015.

[40] R. Zimmerman, C. Murillo-Sánchez, and R. Thomas, "MATPOWER: Steady-state operations, planning and analysis tools for power systems research and education," IEEE Trans. Power Syst., vol. 26, no. 1, pp. 12-19, Feb. 2011.

[41] A. J. Wood and B. F. Wollenberg, *Power Generation Operation and Control*. New York, NY, USA: Wiley, 2003.

[42] A. Farag, S. Al-Baiyat, and T. C. Cheng, "Economic load dispatch multi-objective optimization procedures using linear programming techniques," IEEE Trans Power Syst., vol. 10, no. 2, pp. 731–738, May 1995.

[43] Abido MA. Multi-objective evolutionary algorithms for electric power dispatch problem. IEEE Trans Evol Comput 2006;10(3):315e29.

[44] H. Wang, Z. Lei, X. Zhang, B. Zhou, J. Peng, A review of deep learning for renewable energy forecasting, Energy Conversion and Management, Volume 198, 2019.

[45] X. Lu, K. W. Chan, S. Xia, X. Zhang, G. Wang, F. Li, "A Model to Mitigate Forecast Uncertainties in Distribution Systems Using the Temporal Flexibility of Electric Vehicle Aggregators," IEEE Transactions on Power Systems. Early Access, 2019.

[46] M. Ansari, A. T. Al-Awami, E. Sortomme and M. A. Abido, "Coordinated bidding of ancillary services for vehicle-to-grid using fuzzy optimization," IEEE Transactions on Smart Grid, vol. 6, no. 1, pp. 261-270, Jan. 2015.

[47] Justus. C. G, and Amir Mikhail, "Height variation of wind speed and wind distribution statistics," Geophysics Research Letter, vol. 3, pp. 261-264, 1976.